Characterization, Enrichment, and Computational Modeling of Cross-Linked Actin Networks in Transformed Trabecular Meshwork Cells

Haiyan Li,[1] Devon H. Harvey,[2,3] Jiannong Dai,[2,3] Steven P. Swingle,[4] Anthony M. Compton,[1] Chenna Kesavulu Sugali,[2,3] Kamesh Dhamodaran,[2,3] Jing Yao,[5] Tsai-Yu Lin,[5] Todd Sulchek,[1,4] Taeyoon Kim,[6] C. Ross Ethier,[1,4] and Weiming Mao[2,3,7–9]

[1]Wallace H. Coulter Department of Biomedical Engineering, Georgia Institute of Technology/Emory University, Atlanta, Georgia, United States
[2]Eugene and Marilyn Glick Eye Institute, Indiana University, Indianapolis, Indiana, United States
[3]Department of Ophthalmology, Indiana University, Indianapolis, Indiana, United States
[4]Department of Mechanical Engineering, Georgia Institute of Technology, Atlanta, Georgia, United States
[5]Department of Medical and Molecular Genetics, Indiana University, Indianapolis, Indiana, United States
[6]Weldon School of Biomedical Engineering, Purdue University, West Lafayette, Indiana, United States
[7]Department of Biochemistry & Molecular Biology, Indiana University, Indianapolis, Indiana, United States
[8]Department of Pharmacology and Toxicology, Indiana University, Indianapolis, Indiana, United States
[9]Stark Neurosciences Research Institute, Indiana University, Indianapolis, Indiana, United States

Correspondence: Weiming Mao, RM 305v, 1160 W. Michigan St., Indianapolis, IN 46202, USA; weimmao@iu.edu.

Received: August 17, 2024
Accepted: February 1, 2025
Published: February 26, 2025

Citation: Li H, Harvey DH, Dai J, et al. Characterization, enrichment, and computational modeling of cross-linked actin networks in transformed trabecular meshwork cells. *Invest Ophthalmol Vis Sci.* 2025;66(2):65. https://doi.org/10.1167/iovs.66.2.65

Purpose. Cross-linked actin networks (CLANs) are prevalent in the glaucomatous trabecular meshwork (TM). We previously developed the GTM3L cell line, which spontaneously forms fluorescently labeled CLANs, by transducing GTM3, a transformed glaucomatous TM cell line, with a lentivirus expressing the LifeAct–GFP fusion protein. Here, we determined if LifeAct–GFP viral copy numbers are associated with CLANs, developed approaches to increase CLAN incidence, and computationally studied the biomechanical properties of CLAN-containing GTM3L cells.

Methods. GTM3L cells were fluorescently sorted for viral copy number analysis to determine whether increased CLAN incidence was associated with copy number. CLAN incidence was increased by combining (1) differential adhesion sorting, (2) cell deswelling, and (3) cell stiffness selection. GTM3L cells were cultured on glass or soft hydrogels for stiffness measurement by atomic force microscopy. Computational models studied the biomechanical properties of CLANs.

Results. GTM3L cells had one LifeAct–GFP viral copy/cell on average, and viral copy number or LifeAct–GFP expression level did not associate with CLAN incidence rate. However, CLAN rate was increased from −0.28% to −50% by combining the three enrichment methods noted above. Further, GTM3L cells formed more CLANs on a stiff versus a soft substrate. Computational modeling predicted that CLANs contribute to higher cell stiffness, including increased resistance of the nucleus to tensile stress when CLANs are physically linked to the nucleus.

Conclusions. It is possible to greatly enhance CLAN incidence in GTM3L cells. CLANs are mechanosensitive structures that affect cell biomechanical properties. Further research is needed to determine the biomechanics, mechanobiology, and etiology of CLANs in the TM.

Keywords: GTM3L, trabecular meshwork, cross-linked actin networks, stiffness, computational modeling

Glaucoma, a major cause of blindness, is a common optic neuropathy in which retinal ganglion cell dysfunction and damage result in characteristic patterns of visual field loss. Ocular hypertension (OHT) is a major risk factor for glaucoma; moreover, it is the only treatable risk factor. Ocular hypertension in primary open-angle glaucoma, the most common form of glaucoma, is due to elevated aqueous humor outflow resistance, which in turn is most frequently caused by pathological changes in the trabecular meshwork (TM) and inner wall of Schlemm's canal, as reviewed in Stamer and Clark.[1] Pathological findings in the glaucomatous TM associated with OHT include loss of TM cells,[2–4] compromised TM cell function, excessive extracellular matrix (ECM) deposition, and increased TM[5–7] and ECM stiffness.[6,8] Despite these observations, the fundamental causes of OHT remain unknown.

In addition to the pathological changes described above, it is known that cross-linked actin networks (CLANs) are associated with OHT: they occur more frequently in TM cells from glaucomatous eyes and can be induced by agents known to cause OHT, such as TGF-β2 and dexamethasone (DEX).[9–16] These studies strongly suggest a functional link between CLANs and OHT. CLANs consist of interconnected filamentous (F)-actin ("hub-and-spoke" morphology), appearing as web-like (in two-dimensional images) or spherical (in three-dimensional images) intracellular structures.[11,12] We and others have shown that CLANs colocalize with multiple proteins, including PIP2, syndecan, α-actinin, filamin, PDLIM1, caldesmon, calponin, and tropomyosin.[13,17]

Despite the significant associations between CLANs and OHT/glaucoma, much remains unknown about CLANs, including their impact on cellular functions, ECM production/remodeling, mechanotransduction, and, most importantly, intraocular pressure (IOP). These knowledge gaps are due in part to experimental barriers. For example, it is difficult to induce and visualize CLANs, and thus the reproducibility of CLAN studies has been challenging. Prior to our recent study, most previous CLAN-related research used primary human TM (pHTM) cells together with glucocorticoid, TGF-β2, or integrin activation, with the exception of some studies using bovine TM cells.[11–14,16–20] These approaches have drawbacks; for example, CLAN induction rate varies significantly between cell strains and even between batches from the same cell strain, hindering reproducibility and rigor. Moreover, the use of primary cells is inherently limited by passage numbers,[21] making it challenging to conduct experiments that require a significant number of cells.

We recently described a unique TM cell line, GTM3–LifeAct–GFP (GTM3L).[22] The GTM3L cell line was derived from the widely used GTM3 cell line, established about 20 years ago by immortalizing glaucomatous pHTM cells.[22,23] GTM3 cells share many features with pHTM cells, including phagocytic capability and DEX-inducible myocilin expression.[24–26] We serendipitously discovered the GTM3L subline, which spontaneously forms fluorescently labeled CLANs suitable for live imaging.[22] Using these cells, we showed that CLANs make TM cells stiffer, less dynamic, and more resistant to latrunculin-B (an actin polymerization inhibitor).[22]

Interestingly, not all GTM3L cells form CLANs.[22] To further study CLANs using GTM3L cells, it is important to enrich CLAN$^+$ cells beyond their spontaneous low incidence rate (defined as the number of CLAN$^+$ cells divided by the total number of cells) reported in GTM3L cells.[22] In this study, we explored the association between LifeAct–GFP viral copy numbers/expression levels and CLANs, combined several methods to increase CLAN incidence rate in GMT3L cells with validation of their effects on cell stiffness, and developed a computational model to study the biomechanical impact of CLANs on cells.

Methods

Cell Culture

GTM3L cells were cultured in low-glucose Dulbecco's modified Eagle's medium (DMEM; Gibco, Thermo Fisher Scientific, Waltham, MA, USA) or Opti-MEM (Thermo Fisher Scientific) containing 10% fetal bovine serum (FBS; HyClone, Thermo Fisher Scientific) and 1% penicillin/streptomycin/glutamine (PSG; Gibco/Thermo Fisher Scientific) and maintained at 37°C in a humidified atmosphere with 5% CO_2. Fresh media were supplied every 2 to 3 days. Selection antibiotics/selection pressure was not applied during this study since we observed no obvious loss of LifeAct–GFP expression over time.

Dexamethasone-Induced Myocilin Expression

GTM3L cells were cultured in a 6-well plate. When the cells were close to confluent, medium was changed to serum-free medium containing 0.1% ethanol (EtOH) or 100 nM DEX (Sigma-Aldrich, Saint Louis, MO, USA) for 7 days. Medium was changed once at day 3. At the end of treatment, whole-cell lysates were collected using M-PER buffer (Thermo Fisher Scientific). Protein concentration was estimated using the DC protein assay kit (Bio-Rad, Hercules, CA, USA). Equal amounts of protein were separated on a 10% SDS-PAGE gel and transferred to a PVDF membrane (Bio-Rad). After blocking with the Superblock buffer (Thermo Fisher Scientific), the PVDF membrane was probed with mouse anti-myocilin (cat. MABN866; Sigma) and rabbit anti-GAPDH (cat. 174S; Cell Signaling Technology, Beverly, MA, USA; 1:1000). After incubation with the secondary antibody conjugated with horseradish peroxidase (HRP; Cell Signaling Technology; 1:10,000), signal was developed using the SuperSignal West Femto Maximum Sensitivity Substrate (Thermo Fisher Scientific) and detected using a ChemiDoc imager (Bio-Rad). Densitometry was conducted using ImageJ software (National Institutes of Health [NIH], Bethesda, MD, USA). Briefly, the integrated density of each band was measured. After background subtraction, the expression of myocilin was normalized to GAPDH. The expression level of one of the EtOH-treated samples was set at 1.00 to facilitate comparison.

Fluorescence-Activated Sorting and Lentiviral Copy Number Analysis

About 2×10^7 GTM3L cells were sorted into three groups with high, medium, and low green fluorescent protein (GFP) intensity using a BD FACSAria III Cell Sorter (BD, Franklin Lakes, NJ, USA) at the core facility at Indiana University School of Medicine (Supplementary Fig. S1). These cells were cultured, and DNA was isolated using a Nucelospin kit (Macherey-Nael, Allentown, PA, USA) for viral copy number analysis. The copy number of the lentiviral vector sequence in the Woodchuck Hepatitis Virus Posttranscriptional Regulatory Element was normalized to the copy number of the host cell's ApoB genomic sequence using droplet digital PCR (Bio-Rad). The primers, PCR conditions, and reagents are listed in Supplementary Materials.

Hydrogel Preparation

The hydrogel precursor gelatin methacryloyl (GelMA [6% w/v final concentration]; Advanced BioMatrix, Carlsbad, CA, USA) was mixed with lithium phenyl-2,4,6-trimethylbenzoylphosphinate (0.075% w/v final concentration) photoinitiator (Sigma-Aldrich). Then, 30 µL of the hydrogel solution was pipetted onto Surfasil-coated (Thermo Fisher Scientific) 18-mm × 18-mm square glass coverslips followed by placing 12-mm round silanized glass coverslips on top to facilitate even spreading of the polymer solution. Hydrogels were cross-linked by exposure to UV light (CL-3000 UV Crosslinker; Analytik, Jena, Germany) at 1 J/cm^2. The hydrogel-adhered coverslips were removed with fine-tipped tweezers and placed hydrogel-side

facing up in 24-well culture plates (Corning; Thermo Fisher Scientific).

Osmotic Deswelling of GTM3L Cells

GTM3L cells were seeded at 3×10^4 cells/cm^2 atop either glass coverslips or soft hydrogels and cultured in DMEM with 10% FBS and 1% PSG overnight. Then, GTM3L cells were cultured in DMEM with 1% FBS and 1% PSG and exposed to 2% polyethylene glycol 300 (PEG300; Sigma-Aldrich) for 2 or 5 days.

Cell Area Measurement

GTM3L cells that underwent nine cycles of adhesion-based selection were seeded at 3×10^4 cells/cm^2 on glass coverslips and cultured in DMEM with 10% FBS and 1% PSG overnight. Then, GTM3L cells were cultured in DMEM with 1% FBS and 1% PSG and exposed to 2% PEG300 for 24 hours. Phase contrast images were captured using an EVOS XL Core Imaging System (Thermo FisherScientific, Waltham, MA, USA). Cell area was measured using FIJI software (NIH), with 100 cells per group being analyzed.

Live-Cell Imaging

Live imaging was used to determine how long CLANs persisted in the presence or after PEG300 removal. CLANs were defined as "F-actin–containing cytoskeletal structures with at least one triangulated actin arrangement consisting of actin spokes and at least three identifiable hubs."[18]

GTM3L cells were seeded in either a 35-mm dish with a 0.17-mm-thick glass bottom (World Precision Instruments, Sarasota, FL, USA) or on a glass chip (chip ID: CGF400800F; ARRALYZE—part of LPKF Group, Garbsen, Germany), which was mounted on a 35-mm plastic dish with a 22-mm square cutout in the center. The glass chip contained 512 microwells of 400 µm diameter and 162 microwells of 800 µm diameter. The bottom of the microwell was about 175 µm thick, and the height of the wall of the microwell was about 475 µm. The behaviors of cells on both substrates, including cell growth rate, cell morphology, GFP expression levels, and formation of CLANs, were similar, and the data we present combine experiments from both substrates. The cells were cultured in serum-free Opti-MEM supplemented with 1% glutamine/penicillin/streptomycin. On treatment day 0, the cells were treated with 3% PEG300 (cat. 202371; Sigma-Aldrich). The cells then were monitored daily for the formation of CLANs, which most often formed between treatment days 4 and 6. In some cells, once CLANs were identified, treatment was withdrawn by gently replacing the medium containing 3% PEG300 with fresh culture media without PEG300. In other cells, medium (containing 3% PEG300) was exchanged with fresh medium containing 3% PEG300, and these cells served as a control to account for the potential of photobleaching during live imaging. The cells were immediately transferred to and were maintained in a stage-top incubator (Tokai, Shizuoka-ken, Japan) secured on the stage of a Nikon Eclipse Ti2 inverted microscope (Nikon, Melville, NY, USA) set at 5% CO_2 and 37°C for the duration of live imaging. Time-lapse images were immediately captured using a 40× objective S plan fluor ELWD objective (Nikon). Further images were captured every 30 seconds for the first 2 hours and then every minute for an additional 4 hours, as well as an additional period of 24 hours with images taken every 3 minutes.

Image Analysis

To determine the persistence time of CLANs after PEG300 withdrawal, three to five researchers individually analyzed the captured images. The time at which CLANs were no longer visible was recorded, and the average time over the three to five observers was taken as the persistence time of CLANs. For this part of the study, our definition of visible CLANs was identical to that described above in "Live-Cell Imaging."

Cell Sorting Based on Cell-Substrate Adherence

GTM3L cells were plated in T75 flasks and grown to confluence in DMEM with 10% FBS and 1% PSG. Then, 2 mL of 0.25% trypsin was added and incubated for 2 minutes at 37°C, and nonadherent cells and media were discarded. The remaining adherent cells were then released by adding a further 2 mL of 0.25% trypsin for 30 seconds, adding media to neutralize the trypsin, centrifuging for 10 minutes at 1000 × *g*, and resuspending the pellet in DMEM with 10% FBS and 1% PSG. The cells were then seeded on glass coverslips for testing osmotic deswelling-induced CLAN formation.

Cell Sorting Based on Cell Stiffness

GTM3L cells were selected by stiffness according to an established protocol.[27–31] In brief, 2 mL of a GTM3L cell suspension (1.8×10^6 cells/mL) was passed through a microfluidic device with a narrow channel designed with fourteen 7-µm constrictions angled at 30° that directed the trajectory of cells and thus fractionated cells, depending on their stiffness. This device was made from PDMS (Sylgard 184; Thermo Fisher Scientific) cured on an SU-8 photoresist mold etched using standard photolithography procedures. The day before sorting, devices were passivated with 1% Pluronic F-68 solution (Thermo Fisher Scientific). Cells suspended in flow buffer (culture media with 20% Percoll to provide neutral buoyancy to cells and 0.4 mg/mL DNAse I to avoid DNA-induced blockage if cells lyse) were flowed into the device at 3 to 7 µL/min and collected from the device outlets (each corresponding to a different stiffness), while control samples were taken from unperfused cells. Samples were spun down and resuspended in 150 µL of fresh culture media, and the suspended cells were plated and expanded.

Atomic Force Microscopy

An MFD-3D AFM (Asylum Research, Santa Barbara, CA, USA) was used to make cell stiffness measurements using silicon nitride cantilevers with an attached borosilicate sphere (diameter = 10 µm; nominal spring constant = 0.1 N/m; Novascan Technologies, Ames, IA, USA). Cantilevers were calibrated by measuring the thermally induced motion of the unloaded cantilever before measurements. The indentation depth was limited to 400 nm to avoid substrate effects, and the tip velocity was adjusted to 800 nm/s to avoid viscous effects.[32] Five measurements/cell were conducted, and at least five cells were measured/group. For hydrogel stiffness measurement, a force map covering a 40-µm × 40-µm area (5 × 5 grid of points) was measured. Data from atomic force microscopy (AFM) measurements were fitted to the Hertz model to calculate the effective Young's modulus of the cells, assuming a Poisson's ratio of 0.5.

Investigative Ophthalmology & Visual Science

Immunostaining

GTM3L cells were fixed with 4% paraformaldehyde (Electron Microscopy Sciences, Hatfield, PA, USA) at room temperature for 20 minutes, permeabilized with 0.5% Triton X-100 (Thermo Fisher Scientific), and incubated with Phalloidin-iFluor or 594 (Cell Signaling Technology, Danvers, MA, USA)/DAPI according to the manufacturer's instructions. Coverslips were mounted with ProLong Gold Antifade (Invitrogen) on Superfrost microscope slides (Thermo Fisher Scientific), and fluorescent images were acquired with a Leica DM6 B upright microscope system (Leica Microsystems Inc., Deerfield, IL, USA). Images were captured from at least 10 fields per group, which corresponds to over a thousand cells. The images were subsequently analyzed to determine the percentage of $CLAN^+$ cells, calculated as the ratio of the number of $CLAN^+$ cells to the total number of cells.

Computational Modeling

To simulate CLAN-like networks, we employed our agent-based model with F-actin and actin cross-linking protein (ACP) simplified via cylindrical segments,[33–36] as shown in Supplementary Figure S2. A cell nucleus was included in some simulations, represented as a triangulated mesh. The positions of all points defining the cylindrical segments and the triangulated mesh were updated in each time step using the Langevin equation and the forward Euler integration scheme. For all elements, extensional, bending, and repulsive forces were considered deterministic forces. For the nucleus, forces enforcing conservation of volume and surface area were also considered. F-actins were assembled via nucleation with specific orientations and polymerization, but they did not undergo depolymerization. Actin cross-linking proteins interconnected pairs of F-actins to form functional cross-linking points.

Via the self-assembly process of F-actin and ACP, CLAN-like networks were created. In simulations without the cell nucleus, the CLAN-like network was formed in a thin rectangular domain ($10 \times 8.66 \times 0.1$ µm) with periodic boundary conditions in the x and y directions. The actin concentration (C_A) was chosen to be 100 µM, which is comparable to actin levels in cells,[37] and the molar ratios of ACPs ($R_{ACP} = C_{ACP}/C_A$) were taken as 0.1 to maintain connectivity between F-actins (see Supplementary Materials). After network assembly, the periodic boundary condition was disabled in the y direction. Then, F-actins crossing the two boundaries normal to the y direction were severed, and their ends were clamped to the boundaries. For bulk rheology measurement, the +y boundary was displaced in either the +x, +y, or –y directions at a constant rate to apply shear, tensile, or compressive strain to the network, respectively, while the –y boundary was fixed. The maximum strain was 0.05, and the strain rate was 0.001 s^{-1}. At each strain level, stress was calculated by summing the component of forces acting on the ends of all F-actins clamped on the +y boundary and then dividing the sum by the boundary area. For shear stress, the x component of forces was used, but for tensile and compressive stresses, the y component was used. Simulations with the cell nucleus were performed in a larger rectangular domain with or without the CLAN-like network. For simplicity, the nucleus was simplified as a sphere of diameter 5 µm, although the nucleus generally has an oval shape. The CLAN-like network was created along the nucleus surface as explained earlier, in a three-dimensional rectangular domain ($10 \times 10 \times 5.1$ µm). Note that the initial z dimension of the domain is close to the diameter of the nucleus. The actin structure was created right above the nucleus (i.e., within a space defined by a radial distance from the nucleus center between r_N and $1.1 \times r_N$, where r_N is a nucleus radius). During the actin assembly, the nucleus was frozen without a change in its spherical shape. C_A was 60 µM, which was calculated using the space for actin assembly. R_{ACP} was 0.1 (see Supplementary Materials). It is assumed that 20% of F-actins experience attractive forces from the nucleus to mimic links formed by the linker of nucleoskeleton and cytoskeleton (LINC) complex.[38] After network assembly, compressive strain was applied to the +y boundary, whereas the –y boundary was fixed. The maximum compressive strain was –0.2 (i.e., 20% decrease in the z dimension of the domain), and the strain rate was –0.01 s^{-1}. In each strain level, a total resistant force exerted by the actin structure and the nucleus was measured, and then stress was calculated by dividing the total force by the contact area between the nucleus and the boundary. Further details of the agent-based model and parameters used in simulations are given in Supplementary Materials.

Statistical Analysis

GraphPad Prism software v10.2.3 (GraphPad Software, La Jolla, CA, USA) was used for all analyses. All data sets were tested for normality using the Shapiro–Wilk test and confirmed to meet the normality criteria. The significance level was set at $P < 0.05$. Comparisons between groups were assessed by Student's *t*-tests or one-way analysis of variance with Tukey's multiple comparisons post hoc tests.

Results

GTM3L Cells Had One Viral Insertion per Cell on Average

Although the original GTM3 cells were monoclonal, after lentiviral (pLenti–LifeAct–EGFP–BlastR)[39] transduction and antibiotic selection, GTM3L cells were established to be polyclonal and observed to have variable GFP intensities. We hypothesized this variation was related to different expression levels of the LifeAct–GFP fusion protein and conducted studies to test this hypothesis.

We first confirmed that GTM3L cells showed DEX-induced myocilin expression, a key marker for TM cell characterization,[21] since lentiviral integration might alter cell phenotype. We found that DEX significantly increased myocilin expression, confirming that our GTM3L cells replicate this important feature of TM cell biology (Fig. 1).

We sorted GTM3L cells into three groups with high, medium, and low GFP intensity, respectively (Supplementary Fig. S1). These cells were cultured, and DNA was isolated for viral copy number analysis. We found that naive GTM3 cells had a negligible viral copy number per cell, with readings at background levels. In contrast, all three groups of GTM3L cells had one viral copy per cell on average (Table), regardless of their GFP intensity, suggesting that the number of viral copy/insertions per cell was not correlated with LifeAct–GFP expression levels.

We found that CLAN formation rate was very low among all three groups of GTM3L cells described previously (high, medium, and low GFP intensities) and was similar to unsorted GTM3L cells (data not shown). Since CLANs were

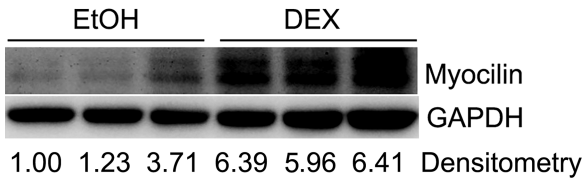

Figure 1. Western immunoblotting showing DEX-induced myocilin expression in GTM3L cells. GTM3L cells were treated with 0.1% EtOH or 100 nM DEX for 7 days. Whole-cell lysate was used for Western immunoblotting to determine the expression of myocilin and GAPDH (loading control). The experiment was conducted in triplicate. Densitometry was conducted and the expression level of myocilin was normalized to GAPDH. A comparison of densitometry values of myocilin shows a significant induction by DEX using the unpaired Student's *t*-test ($n = 3$, $P < 0.05$).

Table. Average Viral Copy Number per GTM3L Cell

Cells	Average Viral Copy Number Per Cell
Naive GTM3 (negative control)	0.0001
GTM3L high GFP intensity	1.0999
GTM3L medium GFP intensity	1.1299
GTM3L low GFP intensity	1.1320

relatively easy to identify in GTM3L cells with medium and high GFP expression, these two groups of cells were used in subsequent studies.

Enrichment of CLAN-Forming Cells Based on Cell-Substrate Adhesion, Osmotic Deswelling, and Cell Stiffness

Enrichment of CLAN$^+$ Cells Based on Cell-Substrate Adhesion. It has been observed that interactions between cells and substrates can enhance the formation of CLANs in TM cells.[17,19,40] We thus reasoned that CLAN$^+$ cells might demonstrate altered adhesion to their substrate. This insight led us to employ an adhesion-based selection strategy to augment the proportion of CLAN$^+$ cells. We noted that after nine cycles of selecting GTM3L cells with stronger substrate attachment, there was a remarkable increase in the frequency of CLAN$^+$ cells, rising from a low incidence of 0.28% ± 0.42% to 4.16% ± 2.95% (Fig. 2A). The CLAN incidence rate in unselected cells was somewhat higher, albeit still small, versus that seen in the original GTM3L cells (0.04%),[22] which is likely due to the use of GTM3-high GFP expression cells (described above).

Enrichment of CLAN$^+$ Cells Using PEG300. Studies have shown that macromolecular crowding induced by PEG promotes CLAN formation in an acellular actin filament solution modeling system.[41,42] We hypothesized that cell shrinkage induced by PEG would also facilitate CLAN formation in GTM3L cells. To investigate the effect of cellular crowding on CLAN formation in GTM3L cells, cells that had undergone nine cycles of adhesion-based selection (see above) were treated with 2% PEG300 for either 2 or 5 days, after which we quantified the incidence rate of CLAN$^+$ cells.

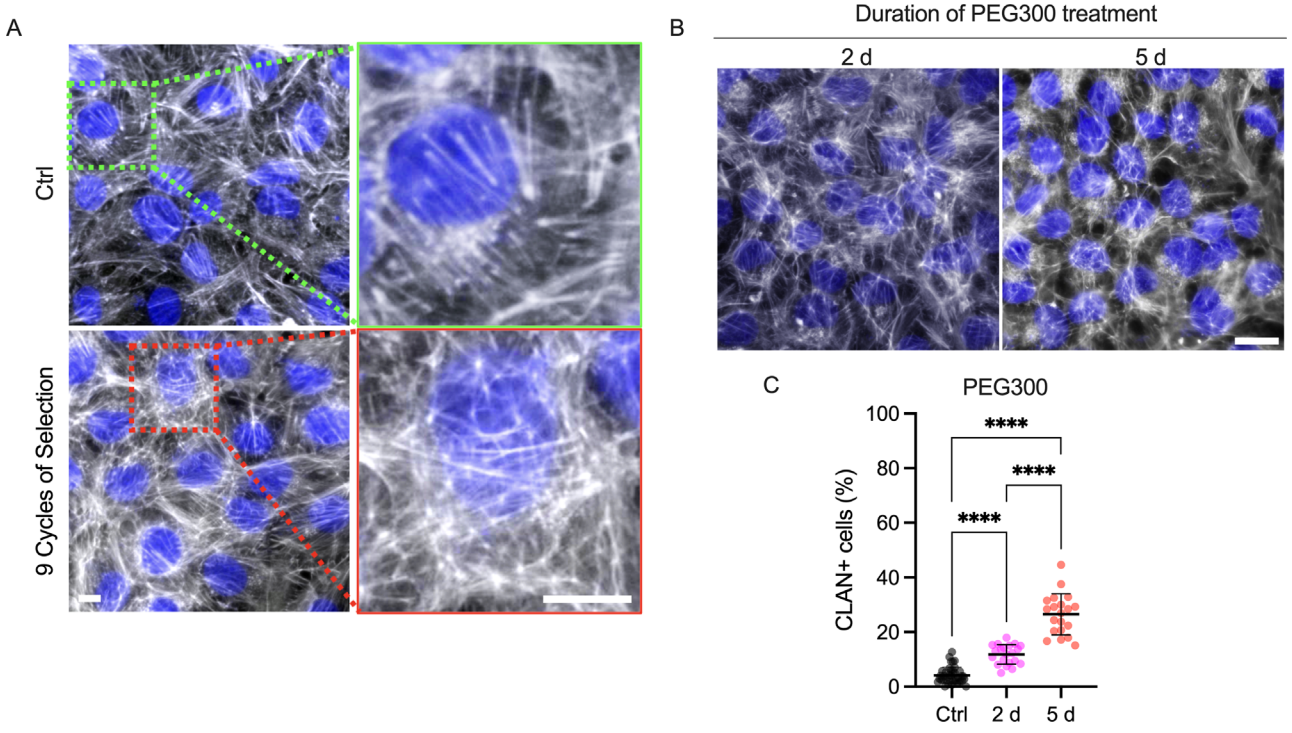

Figure 2. Enrichment of CLAN$^+$ GTM3L cells using adhesion-based selection and PEG300 deswelling. (**A**) Representative fluorescence micrographs of F-actin in GTM3L cells before and after nine cycles of adhesion-based selection, with nuclei (DAPI) and F-actin (Phalloidin–Alexa 555) labeling shown in *blue* and *gray*, respectively. The *green inset* in **A** shows a zoomed-in view of F-actin that does not form a CLAN. The *red inset* in **B** shows a zoomed-in view of F-actin in a CLAN. *Scale bars*: 10 µm. (**B**) Representative fluorescence micrographs of F-actin in GTM3L cells that underwent nine cycles of adhesion-based selection and were then subjected to PEG300 treatment for either 2 or 5 days. Nuclei and F-actin are labeled in *blue* and *gray*, respectively. *Scale bar*: 20 µm. (**C**) Analysis of the percentage of CLAN$^+$ cells caused by treatment with PEG300 for 2 and 5 days ($n = 40$ images from 12 experimental replicates for the control group, $n = 20$ images/group from 6 experimental replicates for the groups treated with 2% PEG300). The *bars* and *error bars* indicate means ± standard deviations. Significance was determined by one-way analysis of variance using multiple comparisons tests. ****$P < 0.0001$.

Investigative Ophthalmology & Visual Science

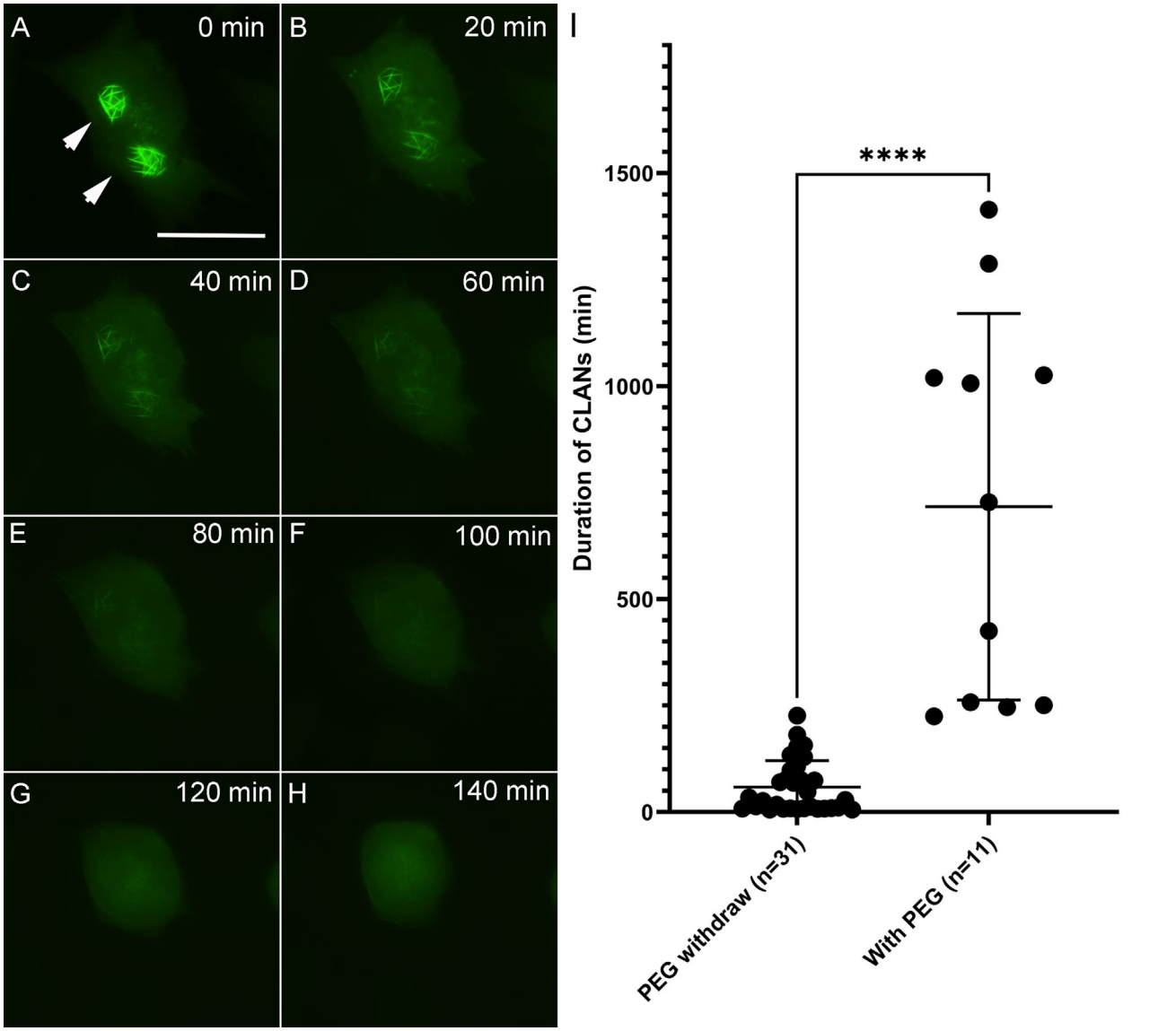

Figure 3. The persistence of CLANs after PEG300 withdrawal. (**A–H**) Images of a GTM3L cell at various times after PEG300 was removed from cells by medium change. *Arrowheads* denote CLANs in live cells. *Scale bar*: 50 µm. (**I**) The persistence time of CLANs after PEG300 withdrawal, as assayed in 31 GTM3L cells (58.9 ± 61.7 minutes), was compared to that of CLANs in the presence of PEG300, as assayed in 11 GTM3L cells (717.1 ± 453.9 minutes). *Bars*: mean and SD. ****$P < 0.0001$ by Student's *t*-test.

As expected, the GTM3L cells exposed to PEG300 shrank, showing a significantly decreased cell area (Supplementary Fig. S3). Additionally, there was a marked increase in the incidence of CLAN$^+$ cells compared to the control group (i.e., versus cells that had been enriched by selecting for adhesion but without PEG300 deswelling) (Fig. 2B). Specifically, the CLAN$^+$ incidence rate was 4.16% ± 2.95% in control cells, which increased to 11.80% ± 3.58% and 26.50% ± 7.51% after 2 and 5 days of PEG300 treatment, respectively (Figs. 2B, 2C).

The Disassembly and Assembly of CLANs. We further studied whether withdrawal of PEG300 would lead to the loss of CLANs. GTM3L cells were treated with PEG300 for 4 to 7 days to induce CLAN formation, followed by replacement of the PEG300-containing culture media with the PEG300-free medium or PEG300-containing media (as a control for potential photobleaching during imaging). We observed a time-dependent loss of CLANs after PEG300 withdrawal (Figs. 3A–H and Supplementary Video S1). Interestingly, while CLAN formation required several days, most of the PEG300-induced CLANs were lost within a few hours after PEG300 withdrawal (CLAN persistence = 58.9 ± 61.7 minutes [mean ± SD], $n = 31$ cells). In contrast, in the continued presence of PEG300, CLANs lasted significantly longer (717.1 ± 453.9 minutes [mean ± SD], $n = 11$ cells; $P < 0.0001$) (Fig. 3I and Supplementary Video S2, cell 1).

Further, during the recording of CLANs in the presence of PEG300 (control studies for photobleaching as described above), we fortuitously recorded the assembly of CLANs in several cells. To our surprise, the assembly/appearance of a CLAN took only a few minutes (Supplementary Video S2 [cell 2], and Supplementary Video S3).

Enrichment of CLAN$^+$ Cells Based on Cell Stiffness. We recently showed that GTM3L cells containing

Investigative Ophthalmology & Visual Science

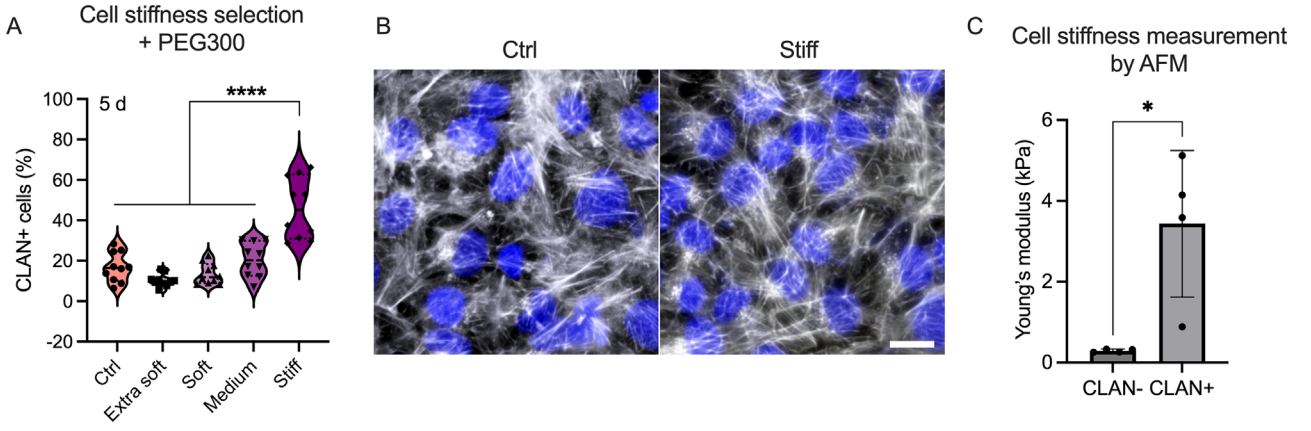

Figure 4. Enrichment of CLAN$^+$ GTM3L cells based on cell stiffness. (**A**) GTM3L cells, after nine cycles of adhesion-based selection, were sorted into four groups according to their stiffness: extra soft, soft, medium, and stiff. Control cells were unsorted cells. Each group of cells was plated on coverslips and exposed to 2% PEG300 for 5 days. The incidence rate of CLAN$^+$ cells was quantified in each cell group (n = 10 images/group from three experimental replicates). The violin plot shows medians as *horizontal solid lines* and the interquartile range as *dashed lines*. Significance was determined by one-way analysis of variance using multiple comparisons tests. ****$P < 0.0001$. (**B**) Representative fluorescence micrographs of F-actin in stiff GTM3L cells that were subjected to PEG300 treatment for 5 days. Nuclei (DAPI) and F-actin (Phalloidin–Alexa 555) are labeled in *blue* and *gray*, respectively. *Scale bar*: 20 µm. (**C**) Stiffness of CLAN$^+$ and CLAN$^-$ cells in an enriched GTM3L cell population was measured by AFM with a 10-µm tip (n = 4 cells/group). The *bars* and *error bars* indicate means ± standard deviations. Significance was determined by unpaired Student's t-test. *$P < 0.05$.

CLANs are stiffer than cells without CLANs.[22] Therefore, we asked whether we could further enrich CLAN$^+$ cells using a well-established microfluidic device that sorts cells depending on their stiffness.[27–31] GTM3L cells, after undergoing nine cycles of adhesion-based selection, were passed through this device, which contains a narrow channel with angled constrictions that direct cells along a stiffness-dependent trajectory, thereby sorting cells into four groups according to their stiffness. There were five outlets in the device, and each outlet admitted cells within a certain stiffness range. We note that no cells were obtained from one of the five outlets and thus have only four groups that we denote as extra soft, soft, medium, and stiff. Note that these categorizations do not map onto cellular Young's modulus values definable a priori, since the sorting process depends on cell stiffness, channel geometry, and cell size and shape.[27–31] To evaluate the capability of these sorted cells to form CLANs, we then subjected them to a 5-day treatment with PEG300, using unsorted cells as a control. We established an association between the stiffness of GTM3L cells, based on microfluidic-based cell sorting, and their ability to form CLANs. Specifically, we observed a significant elevation in CLAN formation as cell stiffness increased (Figs. 4A, 4B).

Together, using a combination of all three CLAN$^+$ cell enrichment methods (nine cycles of adhesion-based selection, cell sorting based on cell stiffness, and PEG300 treatment), we created a GTM3L subpopulation containing about 50% CLAN$^+$ cells (Figs. 4A, 4B). This represents a significant enrichment from the original 0.28% CLAN$^+$ incidence in GTM3L cells.

Confirmation of Cell Stiffening in Enriched GTM3L Cells

Motivated by our previous findings that CLAN$^+$ GTM3L cells are stiffer than CLAN$^-$ GTM3L cells and naive GTM3 cells,[22] we also measured cell stiffness using AFM. We noted that in our current and previous[22] studies, the CLAN$^+$ GTM3L cells were reported to have a stiffness of approximately 4 kPa. Importantly, we confirmed that CLAN$^+$ cells were stiffer than CLAN$^-$ cells (n = 4 cells/group, $P < 0.05$) (Fig. 4C). This strengthens our confidence in our approach to selecting CLAN$^+$ cells from a mixed population.

Substrate Stiffness Influences CLAN Incidence in GTM3L Cells

Substrate stiffness has been shown to affect cell stiffness, with cells adapting by increasing their own stiffness in response to being cultured on a more rigid substrate.[43,44] In our study, we observed a notable correlation between the stiffness of cells and the presence of CLANs. Therefore, we hypothesized that substrate stiffness might also impact the formation of CLANs in GTM3L cells. To explore this hypothesis, we cultured stiff GTM3L cells, enriched through adhesion-based and cell stiffness selection steps (see above), on two different substrates: soft hydrogels with a stiffness of approximately 2.36 kPa and stiff glass coverslips. The cells were then treated with PEG300 for 5 days. We observed that GTM3L cells cultured on the stiff substrate exhibited a significantly elevated incidence of CLAN$^+$ cells ($P < 0.0001$) (Fig. 5).

The Mechanical Properties of CLAN-Like Networks and CLAN-Containing Nucleus

To further study the impact of CLANs on cell biomechanics, we used agent-based models to probe the rheological properties of CLANs and the role of CLANs in cell stiffening. First, we created a CLAN-like network with a triangular lattice geometry (Fig. 6A) and performed bulk rheology measurements imposing shear, tensile, and compressive strains on the network (Fig. 6B). We found that network stiffness was greatest when delivering tensile strain and the smallest when delivering shear strain (Fig. 6B), implying that CLANs in cells resist tensile deformation effectively. Next,

Investigative Ophthalmology & Visual Science

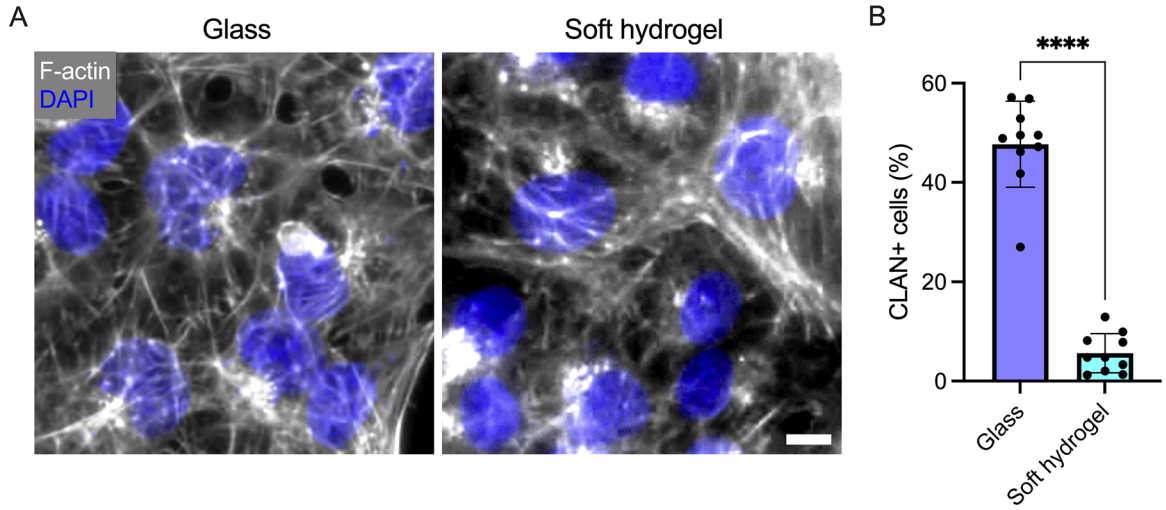

Figure 5. Substrate stiffness affects CLAN formation. (**A**) Representative fluorescence micrographs showing F-actin (stained with Phalloidin–Alexa 555) in GTM3L cells, with CLAN incidence rate enriched through adhesion- and cell stiffness–based selection. Cells were cultured on either glass coverslips or soft hydrogels (2.36 kPa). Nuclei (stained with DAPI) are labeled in *blue*. *Scale bar*: 20 µm. (**B**) Incidence rate of CLAN^{+} cells as a function of substrate stiffness ($n = 10$ images/group from three experimental replicates). The *bars* and *error bars* indicate means ± standard deviations. Significance was determined by unpaired Student's *t*-test. ****$P < 0.0001$.

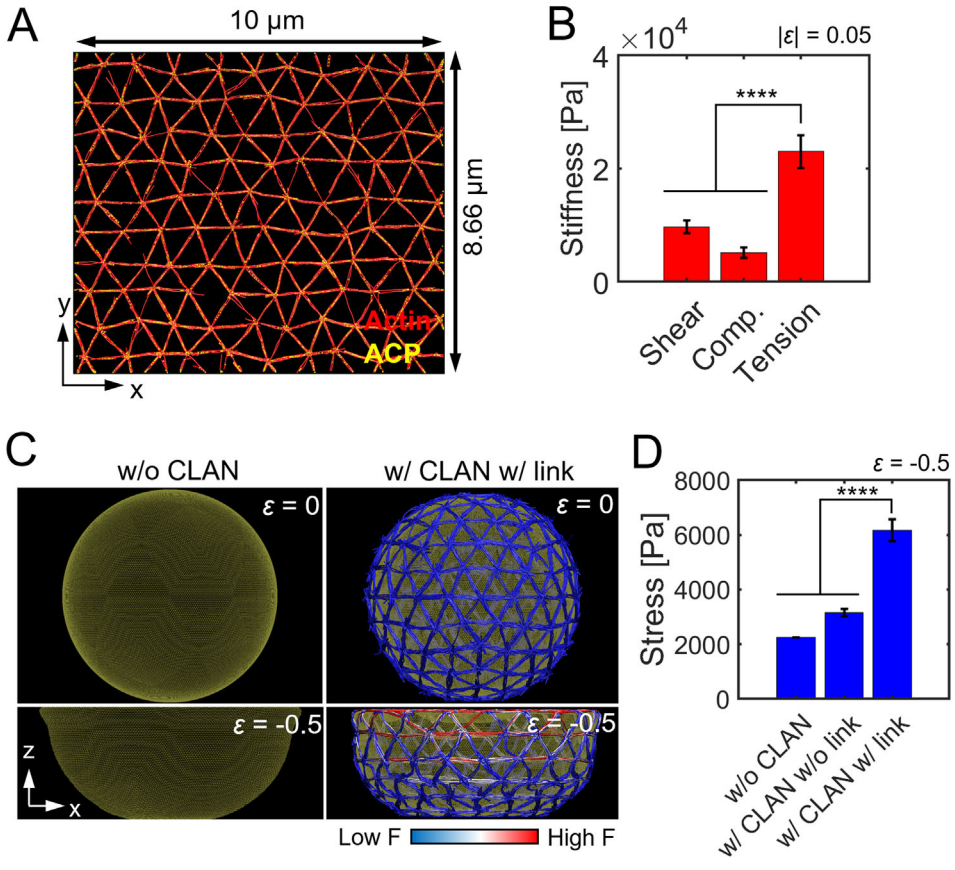

Figure 6. Simulations of the biomechanical effects of CLAN-like networks. (**A**) A CLAN-like network consisting of F-actin (*red*) and ACPs (*yellow*) created in a thin rectangular domain. (**B**) Stiffness of the CLAN-like network in (**A**) in response to shear, tensile, and compressive deformations. The *bars* and *error bars* indicate means ± standard deviations ($n = 10$). Significance was determined by one-way analysis of variance and Tukey post hoc test with $P < 0.0001$ by pairwise comparison between deformation types. (**C**) Snapshots of the nucleus with or without CLANs before and after the application of compressive normal strain up to $\varepsilon = -0.5$. In the case with CLANs, there are physical links between a fraction (20%) of F-actins and the nucleus. Colors in the actin fibers indicate the relative tensile force that fiber is bearing. Compressive forces are considered zero force and shown in *blue*. (**D**) Stress calculated from the resistant force developed during compressive deformations. The *bars* and *error bars* indicate means ± standard deviations ($n = 10$). Significance was determined by one-way analysis of variance and Tukey post hoc test with $P < 0.0001$ by pairwise comparison between conditions.

Investigative Ophthalmology & Visual Science

we performed simulations with only a cell nucleus or with a cell nucleus surrounded by CLANs with or without physical links between the nucleus and CLANs (Figs. 6C, 6D). When compressive strain was applied to the two types of structures, resistance to compression was higher when there were physical links between the nucleus and CLANs (Figs. 6C, 6D). This implies that it is more difficult to deform the nucleus in the presence of CLANs, which is consistent with the increase in cell stiffness measured experimentally by AFM.

Discussion

In this study, we sought to understand various features of the enigmatic actin structures known as CLANs, which occur in TM cells and are associated with ocular hypertension. Toward this end, we used our previously reported GTM3L cells, which spontaneously form GFP-labeled CLANs in some cells. Fortunately, we were able to combine several methods to increase the incidence rate of CLAN$^+$ GTM3L cells, successfully obtaining a subpopulation of GTM3L cells with a −50% CLAN incidence rate. This significant enrichment of CLAN$^+$ cells will be a valuable tool in future work, since it provides a large population of CLAN-positive cells to work with.

We also asked whether the amount of transgene expression in GTM3L cells was associated with the extent of lentiviral integration into the host cell's genome. To our surprise, we found that all GTM3L cells, regardless of their transgene expression levels, had on average only one lentiviral insertion/integration event per cell. Generally, lentiviral integration sites in host chromosomes are random, and a high dose of lentiviruses (more than one copy per cell) can insert at multiple regions in the host cell genome.[45,46]

The above finding led us to the hypothesis that the presence or absence of CLANs in GTM3L cells depends on the locus of lentiviral insertion rather than the number of insertions. The rationale for this hypothesis includes the following:

- It is well known that lentiviruses integrate at random sites as well as at certain "hot spots" in the genome. Since the original GTM3 cells are monoclonal and all GTM3L cells were cultured in the same extracellular environment, the most likely explanation for CLAN formation is the difference in lentiviral integration sites.
- Different from the monoclonal GTM3 cells, our GTM3L cells are polyclonal (i.e., we did not conduct clonal selection or expansion after transduction). We observed a very low and unpredictable CLAN formation rate in GTM3L cells: sometimes there were many CLAN$^+$ cells in a well, and sometimes there were no CLAN$^+$ cells at all. This observation is consistent with our hypothesis and suggests that only a few lentiviral integration patterns will trigger CLAN formation.

Overall, the formation of CLANs in GTM3L cells may require two "hits." We hypothesized that GTM3L cells with certain lentiviral insertion/integration pattern(s) are prone to form CLANs. When these cells grow in an unfavorable environment for CLAN formation, they form only a few CLANs (−0.28%), yet if they grow in a favorable environment, such as on a stiff substrate or in the presence of PEG300, they form significantly more CLANs.

We were able to enrich the population of CLAN$^+$ cells using different methods: differential substrate adhesion, PEG300 exposure, and cell stiffness–based sorting. Interestingly, these methods were synergistic, suggesting that they might be selecting for different CLAN-associated phenotypes. The time scale associated with PEG300 exposure was noteworthy, since the induction of CLANs by PEG300 took several days of exposure, yet CLAN disassembly after PEG300 removal occurred within hours. Interestingly, even though it took CLANs several days to be induced, the actual assembly of CLANs occurred within minutes (Supplementary Video S2 [cell 2] and Supplementary Video S3). We note that two cells we show movies of changed their morphology from elongated to round before CLANs started to form. However, we have seen CLANs in both elongated and rounded GTM3L cells after PEG300 treatment, so a rounded cell shape does not appear to be a prerequisite for CLAN formation. Our current observations of cell morphologic changes before CLAN assembly may be due to our small sample size (only two cells) and/or prolonged preexposure to UV during imaging, which could lead to some cell damage. We also noticed that the intensity of fluorescence decreased rapidly after CLAN disassembly in those cells, which could be due to (1) the cells becoming senescent or entering the process of cell death after UV exposure and/or (2) focus drifting over time.

Although these results are intriguing, there is much that we do not understand about them. Why are CLAN induction and disassembly durations so different? Why are there significant morphologic and fluorescence intensity changes associated with CLAN assembly and disassembly in some cells? What is the exact mechanism by which PEG300 induces CLANs in TM cells? Regarding the last question, the simplest possibility is that cell deswelling by PEG300 leads to cytoplasmic molecular crowding, an effect that was seen in an acellular model where crowding decreased α-actinin binding to F-actin and possibly led to F-actin thinning and shortening.[42] Another possibility is that PEG300 exposure leads to cellular stress and that CLAN formation is a generic stress response of TM cells. For example, the formation of CLANs at the perinuclear region might provide TM cells with additional mechanical shielding or stabilization. This idea that CLANs are a stress response may also help explain the observation that CLANs tend to form more on stiffer substrates, as well as in the presence of DEX and TGF-β2. Overall, our data suggest that CLANs are likely more dynamic than we had previously thought. More experiments are clearly needed to explore this concept and address the open questions listed above.

TM cells can sense substrate stiffness via focal adhesions (FAs) and actomyosin contractility.[47] Myosin motors exert contractile forces to FAs by interacting with F-actins, and a stiffer substrate leads to the development of larger tensile forces on FAs. Then, FAs can be matured with an increase in their size and lifetime via the recruitment of additional integrins. Forces developed on F-actins in a stable manner via matured FAs can be transmitted to the nucleus via physical links between the nucleus and F-actins, such as LINC complex.[48] In case of stress fibers, perinuclear stress fibers that wrap around the nucleus are known to transmit significant forces to the nucleus.[49] Considering that CLANs are often found around the nucleus, it is expected that there would be strong force transmission between them.

We employed an agent-based computational model to understand why CLAN$^+$ cells are stiffer. We hypothesized that CLAN$^+$ cells exhibit higher stiffness because their nuclei are harder to deform due to the surrounding CLANs. To test this hypothesis, we first computationally measured the rheo-

Investigative Ophthalmology & Visual Science

logical properties of CLAN-like networks and found that the networks resisted tensile deformation effectively. Then, we applied compressive deformation to a simplified cell nucleus with or without CLANs and found that the presence of CLANs resulted in much higher resistance of the cell nucleus to compression due to high tensile resistance of CLANs; specifically, deformation of the cell nucleus was hindered by the limited extensibility of actin fibers. Based on these observations, which are consistent with our hypothesis, it is likely that the higher stiffness of CLAN$^+$ cells partially originates from CLANs around the nucleus. Note that we employed a spherical shape for the nucleus for simplicity, instead of the ellipsoidal shape typically observed in cells. However, we expect that the effects of CLANs in limiting nuclear deformation would be similar even if we use the oval-shaped nucleus in simulations. Specifically, CLANs surrounding the nucleus would still resist increases in the dimensions of the nucleus in the x and y directions induced by a change in the z dimension even if the shape of the nucleus was ellipsoidal.

CLANs may also be a downstream response to mechanosignaling by the focal adhesion complex, which is consistent with our understanding that changes in ECM properties (such as ECM stiffness) can cause nuclear deformation via the cytoskeleton. Indeed, TM cells can sense substrate stiffness and deformation via FAs and actomyosin contractility.[50] In general, myosin motors exert contractile forces on FAs by interacting with F-actins, and a stiffer substrate leads to the development of larger tensile forces on FAs. This, in turn, can cause FAs to mature, with an increase in their size and lifetime via the recruitment of additional integrins. Forces developed on F-actin in a stable manner via matured FAs can in turn be transmitted to the nucleus via physical links between the nucleus and F-actin, such as the LINC complex.[38] In the case of stress fibers, perinuclear stress fibers that wrap around the nucleus are known to transmit significant forces to the nucleus.[51] Considering that CLANs are often found around the nuclear region, it is expected that there would be a strong influence of CLANs on force transmission from FAs to the nucleus.

Probably the most important question about CLANs is whether they directly contribute to decreased outflow facility and hence elevated IOP or are simply an associated epiphenomenon. Our data do not directly answer this question; even the finding that a stiff substrate, such as seen in the TM of ocular hypertensive eyes, promotes CLAN formation is consistent with both possibilities. To address this question will require more work in a variety of models, and we suggest that our findings can play an important role by motivating and facilitating cell-based models. For example, one possibility would be to decellularize TM tissue in perfused anterior segments and then repopulate the TM by magnetically steering CLAN$^+$ cells into the TM. Another approach would be to use an artificial outflow pathway construct (TM-on-a-chip), populating the construct with CLAN$^+$ cells to determine effects on flow resistance. All such studies will require large numbers of CLAN$^+$ cells, the production of which will be greatly facilitated by our enrichment strategies. Also, if the gene(s) that promotes CLAN formation is discovered (e.g., by comparing CLAN$^-$ versus CLAN$^+$ GTM3L cells using DNA sequencing), CLAN formation can be induced in the mouse TM and the effect of CLANs on outflow facility and IOP can be determined in vivo.

Of course, this work is subject to certain limitations. Besides the lack of outflow facility and IOP data, key among these is that the GTM3L cells are derived from a transformed cell line (GTM cells). It is well known that the biology of transformed TM cells is different from primary TM cells.[21] However, we believe these GTM3L are still a valuable tool for studying CLANs because of several reasons.

1. Important features are consistent between GTM3L CLAN$^+$ cells and pHTM CLAN$^+$ cells, such as resistance to actin relaxing reagents[16,22] and increased cell stiffness.[22]
2. Our GTM3L cells form CLANs spontaneously, offering several advantages:
   - Live imaging of CLAN$^+$ cells under physiologic conditions.
   - Enriched CLAN$^+$ GTM3L cell populations make omics-based studies possible.
   - Our GTM3L cell line has unlimited proliferation capability, and CLAN formation in this line is spatially consistent (predominantly in the perinuclear region), which improves reproducibility.
3. LifeAct–GFP expression does not affect TM cell biomechanical properties. Unlike human mesenchymal stem cells,[52] our GTM3L cells did not demonstrate adverse effects since CLAN$^-$ GTM3L cells and GTM3 cells showed similar stiffness and viscosity.
4. Our cell culture studies are directly intellectually linked to functional outcomes in whole eyes. Specifically, we know that increased TM tissue stiffness is associated with OHT in glaucomatous eyes[5,6] and impaired IOP homeostasis, which, given the greater stiffness of GTM3L CLAN$^+$ cells, strongly suggests mechanistic link(s) between CLANs and OHT. In the future, we fully expect to be able to translate our findings from GTM3L cells into whole eyes.

In summary, we have developed an effective strategy to greatly increase the presence of CLAN$^+$ cells in our newly discovered GTM3L subline. Based on our findings, we believe that CLANs, induced by glaucomatous signals (elevated TGFβ2, elevated cortisone or steroid treatment, or elevated IOP/mechanical stretching) or even as a primary initiating factor of glaucoma, lead to pathologic changes in TM cell biology, biomechanics, and mechanobiology, resulting in OHT in glaucomatous eyes. Further research is needed to determine these changes and the underlying mechanisms, and this subline will be a useful tool for this purpose.

Acknowledgments

The authors thank Kenneth Cornetta of the Gene Therapy Testing Laboratory at Indiana University School of Medicine for ddPCR resources.

Supported by the National Institutes of Health/National Eye Institute Award Numbers R01EY026962 (WM), R01EY031700 (WM), R21EY033929 (WM), and R01EY031710 (CRE); BrightFocus Foundation G2023009S (WM); a challenge grant from Research to Prevent Blindness (Department of Ophthalmology, Indiana University School of Medicine); the Georgia Research Alliance (CRE); and National Science Foundation Award Number 2134701 (TS) and CBET-2225476 (TS).

The content is solely the responsibility of the authors and does not necessarily represent the official views of the National Institutes of Health.

Disclosure: **H. Li**, None; **D.H. Harvey**, None; **J. Dai**, None; **S.P. Swingle**, None; **A.M. Compton**, None; **C.K. Sugali**, None; **K. Dhamodaran**, None; **J. Yao**, None; **T.-Y. Lin**, None;

T. Sulchek, None; **T. Kim**, None; **C.R. Ethier**, None; **W. Mao**, None

References

1. Stamer WD, Clark AF. The many faces of the trabecular meshwork cell. *Exp Eye Res*. 2017;158:112–123.
2. Alvarado J, Murphy C, Juster R. Trabecular meshwork cellularity in primary open-angle glaucoma and nonglaucomatous normals. *Ophthalmology*. 1984;91:564–579.
3. Grierson I, Howes RC. Age-related depletion of the cell population in the human trabecular meshwork. *Eye (Lond)*. 1987;1(pt 2):204–210.
4. Kuehn MH, Vranka JA, Wadkins D, Jackson T, Cheng L, Ledolter J. Circumferential trabecular meshwork cell density in the human eye. *Exp Eye Res*. 2021;205:108494.
5. Last JA, Pan T, Ding Y, et al. Elastic modulus determination of normal and glaucomatous human trabecular meshwork. *Invest Ophthalmol Vis Sci*. 2011;52:2147–2152.
6. Raghunathan VK, Benoit J, Kasetti R, et al. Glaucomatous cell derived matrices differentially modulate nonglaucomatous trabecular meshwork cellular behavior. *Acta Biomater*. 2018;71:444–459.
7. Vahabikashi A, Gelman A, Dong B, et al. Increased stiffness and flow resistance of the inner wall of Schlemm's canal in glaucomatous human eyes. *Proc Natl Acad Sci USA*. 2019;116:26555–26563.
8. Raghunathan VK, Morgan JT, Park SA, et al. Dexamethasone stiffens trabecular meshwork, trabecular meshwork cells, and matrix. *Invest Ophthalmol Vis Sci*. 2015;56:4447–4459.
9. Tripathi RC, Li J, Chan WF, Tripathi BJ. Aqueous humor in glaucomatous eyes contains an increased level of TGF-beta 2. *Exp Eye Res*. 1994;59:723–727.
10. Armaly MF, Becker B. Intraocular pressure response to topical corticosteroids. *Fed Proc*. 1965;24:1274–1278.
11. Clark AF, Miggans ST, Wilson K, Browder S, McCartney MD. Cytoskeletal changes in cultured human glaucoma trabecular meshwork cells. *J Glaucoma*. 1995;4:183–188.
12. Clark AF, Wilson K, McCartney MD, Miggans ST, Kunkle M, Howe W. Glucocorticoid-induced formation of cross-linked actin networks in cultured human trabecular meshwork cells. *Invest Ophthalmol Vis Sci*. 1994;35:281–294.
13. Bermudez JY, WH PG, Yan LJ, Clark AF, Mao W. Two-dimensional differential in-gel electrophoresis (2D-DIGE) reveals proteins associated with cross-linked actin networks in human trabecular meshwork cells. *J Clin Exp Ophthalmol*. 2016;7(4).
14. Hoare MJ, Grierson I, Brotchie D, Pollock N, Cracknell K, Clark AF. Cross-linked actin networks (CLANs) in the trabecular meshwork of the normal and glaucomatous human eye in situ. *Invest Ophthalmol Vis Sci*. 2009;50:1255–1263.
15. O'Reilly S, Pollock N, Currie L, Paraoan L, Clark AF, Grierson I. Inducers of cross-linked actin networks in trabecular meshwork cells. *Invest Ophthalmol Vis Sci*. 2011;52:7316–7324.
16. Montecchi-Palmer M, Bermudez JY, Webber HC, Patel GC, Clark AF, Mao W. TGFbeta2 induces the formation of cross-linked actin networks (CLANs) in human trabecular meshwork cells through the Smad and non-Smad dependent pathways. *Invest Ophthalmol Vis Sci*. 2017;58:1288–1295.
17. Filla MS, Woods A, Kaufman PL, Peters DM. Beta1 and beta3 integrins cooperate to induce syndecan-4-containing cross-linked actin networks in human trabecular meshwork cells. *Invest Ophthalmol Vis Sci*. 2006;47:1956–1967.
18. Wade NC, Grierson I, O'Reilly S, et al. Cross-linked actin networks (CLANs) in bovine trabecular meshwork cells. *Exp Eye Res*. 2009;89:648–659.
19. Filla MS, Schwinn MK, Nosie AK, Clark RW, Peters DM. Dexamethasone-associated cross-linked actin network formation in human trabecular meshwork cells involves beta3 integrin signaling. *Invest Ophthalmol Vis Sci*. 2011;52:2952–2959.
20. Filla MS, Clark R, Peters DM. A syndecan-4 binding peptide derived from laminin 5 uses a novel PKCepsilon pathway to induce cross-linked actin network (CLAN) formation in human trabecular meshwork (HTM) cells. *Exp Cell Res*. 2014;327:171–182.
21. Keller KE, Bhattacharya SK, Borras T, et al. Consensus recommendations for trabecular meshwork cell isolation, characterization and culture. *Exp Eye Res*. 2018;171:164–173.
22. Peng M, Rayana NP, Dai J, et al. Cross-linked actin networks (CLANs) affect stiffness and/or actin dynamics in transgenic transformed and primary human trabecular meshwork cells. *Exp Eye Res*. 2022;220:109097.
23. Pang IH, Shade DL, Clark AF, Steely HT, DeSantis L. Preliminary characterization of a transformed cell strain derived from human trabecular meshwork. *Curr Eye Res*. 1994;13:51–63.
24. Jain A, Wordinger RJ, Yorio T, Clark AF. Spliceosome protein (SRp) regulation of glucocorticoid receptor isoforms and glucocorticoid response in human trabecular meshwork cells. *Invest Ophthalmol Vis Sci*. 2012;53:857–866.
25. Chen W, Yang X, Fang J, Zhang Y, Zhu W, Yang X. Rho-associated protein kinase inhibitor treatment promotes proliferation and phagocytosis in trabecular meshwork cells. *Front Pharmacol*. 2020;11:302.
26. Gasull X, Castany M, Castellanos A, et al. The LRRC8-mediated volume-regulated anion channel is altered in glaucoma. *Sci Rep*. 2019;9:5392.
27. Islam M, Brink H, Blanche S, et al. Microfluidic sorting of cells by viability based on differences in cell stiffness. *Sci Rep*. 2017;7:1997.
28. Wang G, Mao W, Byler R, et al. Stiffness dependent separation of cells in a microfluidic device. *PLoS One*. 2013;8:e75901.
29. Stone NE, Raj A, Young KM, et al. Label-free microfluidic enrichment of cancer cells from non-cancer cells in ascites. *Sci Rep*. 2021;11:18032.
30. Islam M, Mezencev R, McFarland B, et al. Microfluidic cell sorting by stiffness to examine heterogenic responses of cancer cells to chemotherapy. *Cell Death Dis*. 2018;9:239.
31. Wang G, Turbyfield C, Crawford K, Alexeev A, Sulchek T. Cellular enrichment through microfluidic fractionation based on cell biomechanical properties. *Microfluid Nanofluidics*. 2015;19:987–993.
32. Vargas-Pinto R, Gong H, Vahabikashi A, Johnson M. The effect of the endothelial cell cortex on atomic force microscopy measurements. *Biophys J*. 2013;105:300–309.
33. Li J, Biel T, Lomada P, Yu Q, Kim T. Buckling-induced F-actin fragmentation modulates the contraction of active cytoskeletal networks. *Soft Matter*. 2017;13:3213–3220.
34. Jung W, Murrell MP, Kim T. F-actin cross-linking enhances the stability of force generation in disordered actomyosin networks. *Comput Part Mech*. 2015;2:317–327.
35. Kim T, Hwang W, Lee H, Kamm RD. Computational analysis of viscoelastic properties of crosslinked actin networks. *PLoS Comp Biol*. 2009;5:e1000439.
36. Mak M, Zaman MH, Kamm RD, Kim T. Interplay of active processes modulates tension and drives phase transition in self-renewing, motor-driven cytoskeletal networks. *Nat Commun*. 2016;7:10323.
37. Kiuchi T, Nagai T, Ohashi K, Mizuno K. Measurements of spatiotemporal changes in G-actin concentration reveal its effect on stimulus-induced actin assembly and lamellipodium extension. *J Cell Biol*. 2011;193:365–380.

Investigative Ophthalmology & Visual Science

38. Bouzid T, Kim E, Riehl BD, et al. The LINC complex, mechanotransduction, and mesenchymal stem cell function and fate. *J Biol Eng*. 2019;13:68.
39. Padilla-Rodriguez M, Parker SS, Adams DG, et al. The actin cytoskeletal architecture of estrogen receptor positive breast cancer cells suppresses invasion. *Nat Commun*. 2018;9:2980.
40. Filla MS, Schwinn MK, Sheibani N, Kaufman PL, Peters DM. Regulation of cross-linked actin network (CLAN) formation in human trabecular meshwork (HTM) cells by convergence of distinct beta1 and beta3 integrin pathways. *Invest Ophthalmol Vis Sci*. 2009;50:5723–5731.
41. Huber F, Strehle D, Schnauß J, Käs J. Formation of regularly spaced networks as a general feature of actin bundle condensation by entropic forces. *N J Phys*. 2015;17:043029.
42. Park J, Lee M, Lee B, Castaneda N, Tetard L, Kang EH. Crowding tunes the organization and mechanics of actin bundles formed by crosslinking proteins. *FEBS Lett*. 2021;595:26–40.
43. Janmey PA, Fletcher DA, Reinhart-King CA. Stiffness sensing by cells. *Physiol Rev*. 2020;100:695–724.
44. Solon J, Levental I, Sengupta K, Georges PC, Janmey PA. Fibroblast adaptation and stiffness matching to soft elastic substrates. *Biophys J*. 2007;93:4453–4461.
45. Mitchell RS, Beitzel BF, Schroder AR, et al. Retroviral DNA integration: ASLV, HIV, and MLV show distinct target site preferences. *PLoS Biol*. 2004;2:E234.
46. Schroder AR, Shinn P, Chen H, Berry C, Ecker JR, Bushman F. HIV-1 integration in the human genome favors active genes and local hotspots. *Cell*. 2002;110:521–529.
47. Oakes PW, Gardel ML. Stressing the limits of focal adhesion mechanosensitivity. *Curr Opin Cell Biol*. 2014;30:68–73.
48. King MC. Dynamic regulation of LINC complex composition and function across tissues and contexts. *FEBS Lett*. 2023;597:2823–2832.
49. Alisafaei F, Jokhun DS, Shivashankar GV, Shenoy VB. Regulation of nuclear architecture, mechanics, and nucleocytoplasmic shuttling of epigenetic factors by cell geometric constraints. *Proc Natl Acad Sci USA*. 2019;116:13200–13209.
50. Hayakawa K, Tatsumi H, Sokabe M. Mechano-sensing by actin filaments and focal adhesion proteins. *Commun Integr Biol*. 2012;5:572–577.
51. Maninova M, Vomastek T. Dorsal stress fibers, transverse actin arcs, and perinuclear actin fibers form an interconnected network that induces nuclear movement in polarizing fibroblasts. *FEBS J*. 2016;283:3676–3693.
52. Flores LR, Keeling MC, Zhang X, Sliogeryte K, Gavara N. Lifeact-GFP alters F-actin organization, cellular morphology and biophysical behaviour. *Sci Rep*. 2019;9:3241.

Investigative Ophthalmology & Visual Science